THE ASTROPHYSICAL JOURNAL, 287:359–370, 1984 December 1

ROCKET OBSERVATIONS OF THE ORION REFLECTION NEBULOSITY IN THE RANGE 130–200 NANOMETERS AND SCATTERING PROPERTIES OF DUST GRAINS IN THE FAR-ULTRAVIOLET

TAKASHI ONAKA, MINEO SAWAMURA, AND WATARU TANAKA
Department of Astronomy, University of Tokyo
AND
TETSUYA WATANABE AND KEIICHI KODAIRA
Tokyo Astronomical Observatory
Received 1983 December 13; accepted 1984 June 18

ABSTRACT

Vacuum ultraviolet surface brightness maps of the southern part of the Orion region at the wavelengths 195.1, 179.6, 164.0, 148.4, and 132.8 nm were obtained by a rocket experiment. Large-scale bright nebulosity and a ridge structure in the western circumference of the Orion regions are clearly seen in these contour maps. They are interpreted as diffuse reflection of starlight by dust grains. The effective albedo of the scattering layer increases from 195.1 to 179.6 nm but does not change appreciably in the 179.6–148.4 nm range. The radial gradient of the spatial distribution is almost constant in the 195.1–148.4 nm range, with a slight decrease at 164.0 nm. Simple analysis shows that the observations can be explained by a front-dust-layer model, in which the diffuse light arises from the starlight scattered by dust grains in front of the stars, as well as by a back-dust-layer model, where dust grains behind the stars scatter the starlight to produce the diffuse nebulosity. The decrease in the radial gradient at 164.0 nm and the spectral property of the radiation from the ridge structure can be favorably interpreted by the model with front and side dust layers. It is also indicated that a scattering phase function of the involved dust grains does not necessarily have a less forward-scattering form around 150 nm than around 190 nm, which was suggested by previous investigators. However, regardless of the assumed geometry, the ultraviolet phase function in Orion is less forward scattering than is the commonly accepted phase function near 500 nm. Implications of the suggested scattering properties are discussed in relation to the dust model in the far-ultraviolet region.

Subject headings: interstellar: grains — nebulae: Orion Nebula — ultraviolet: general

I. INTRODUCTION

The identification of interstellar solid particles is one of the most important problems in present-day astrophysics (cf. Savage and Mathis 1979). Most model analyses have been based on the spectral dependence of interstellar extinction (see Mathis, Rumpl, and Nordsieck 1977). Interstellar polarization gives additional restrictions to the identification (Martin 1972; Hong and Greenberg 1978, 1979; Aannestad and Greenberg 1983). The scattering properties of grains deduced from observations of diffuse background light can also provide significant evidence for proposed material (see Lillie and Witt 1976).

The subject of the present study, the Orion reflection nebulosity, is one of the objects that have been investigated intensively in this context. Photographs have shown that ultraviolet diffuse flux spreads widely over the Orion region (O'Dell, York, and Henize 1967, hereafter OYH; Carruthers and Opal 1977*a*, *b*). An amorphous ring structure including the Barnard Loop is seen in the 220–410 nm passband (OYH) and is hard to distinguish from the large-scale nebulosity in the 270–150 nm passbands (Morgan, Nandy, and Thompson 1982, hereafter MNT). The large-scale nebulosity has been interpreted as reflection of the light from blue Orion stars by dust grains lying behind them (Witt and Lillie 1978; MNT).

In §§ II and III, we present our recent photometric observations of the southern part of the Orion reflection nebulosity in the vacuum ultraviolet region, carried out by a rocket experiment (Tanaka *et al.* 1984, hereafter Paper I). Our observations have a spatial resolution comparable to that of the previous observations and have a higher spectral resolution than those observations, thus giving additional detailed information about dust properties. In § IV, we calculate dust-layer models with two different geometries: backscattering by dust grains behind the illuminating stars and forward scattering by grains in front of the stars. A ridge structure of diffuse light around $\alpha \approx 5^h23^m$, which appears clearly after the subtraction of the large-scale nebulosity components, is also examined in terms of dust scattering. The resulting scattering properties are discussed in § V in relation to the present observations and those of interstellar extinction.

II. OBSERVATIONS

The data were obtained with a five-band spectrophotometer carried aboard the attitude-controlled S520-3 sounding rocket of the Institute of Space and Astronautical Science (ISAS), Japan, on 1982 February 14. The southern Orion region, $8° \times 8°$ centered at $\alpha = 5^h30^m$ and $\delta = -4°$ (1950.0), was raster-scanned three times with a 16′ field of view. The spectrophotometer consists of a 30 cm modified Cassegrain system, a concave grating, and five photomultipliers operating in photon-counting mode, each corresponding to the central wavelength, 132.8, 148.4, 164.0, 179.6, or 195.1 nm. The bandwidth was 4.2 nm in half-width for all passbands. The system was calibrated prior to the flight. The stray light was considered to be negligible at the levels in question because of the deep sky baffles and the careful photometer design. Full details

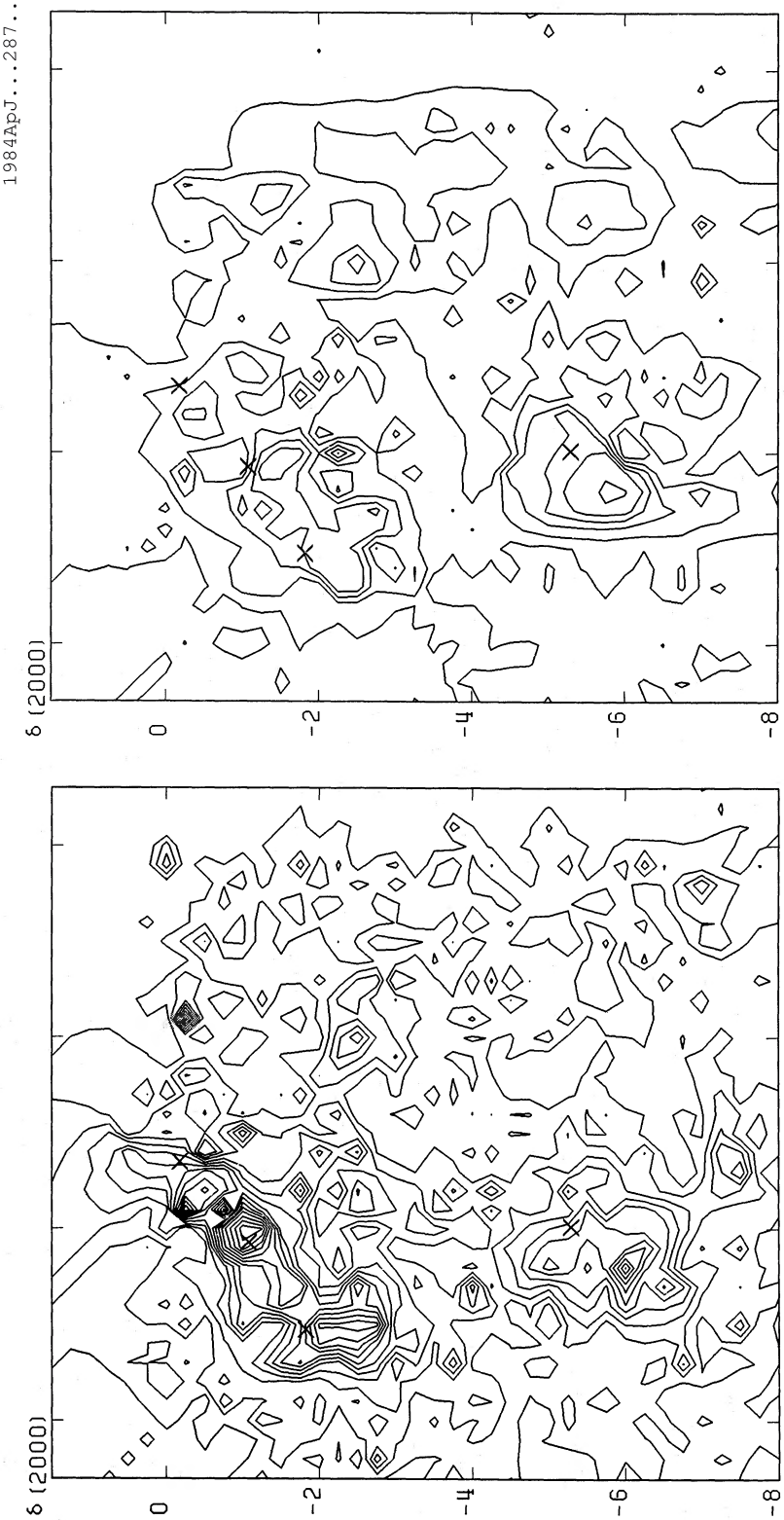

FIG. 1a

FIG. 1b

FIG. 1.—Contour maps of the Orion reflection nebulosity at (*a*) 148.4 nm, (*b*) 164.0 nm, (*c*) 179.6 nm, and (*d*) 195.1 nm. Contours run in increments of 1×10^{-7} ergs cm^{-2} sec^{-1} sr^{-1} Å^{-1} up to 2×10^{-6} ergs cm^{-2} sec^{-1} sr^{-1} Å^{-1}. Crosses represent the locations of θ Ori, ζ Ori, ϵ Ori, and δ Ori in order of declination.

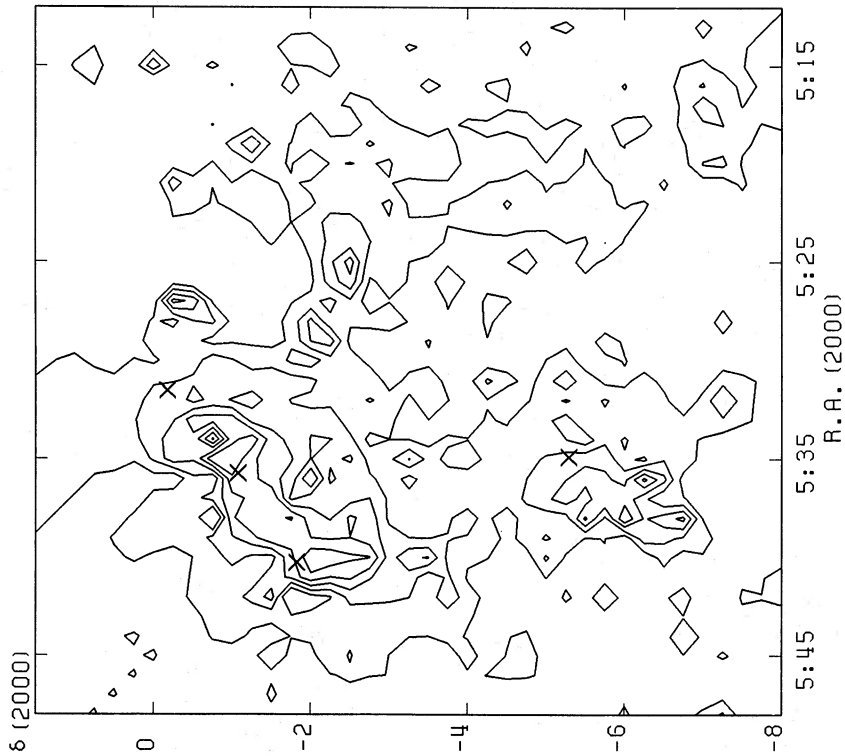

FIG. 1d

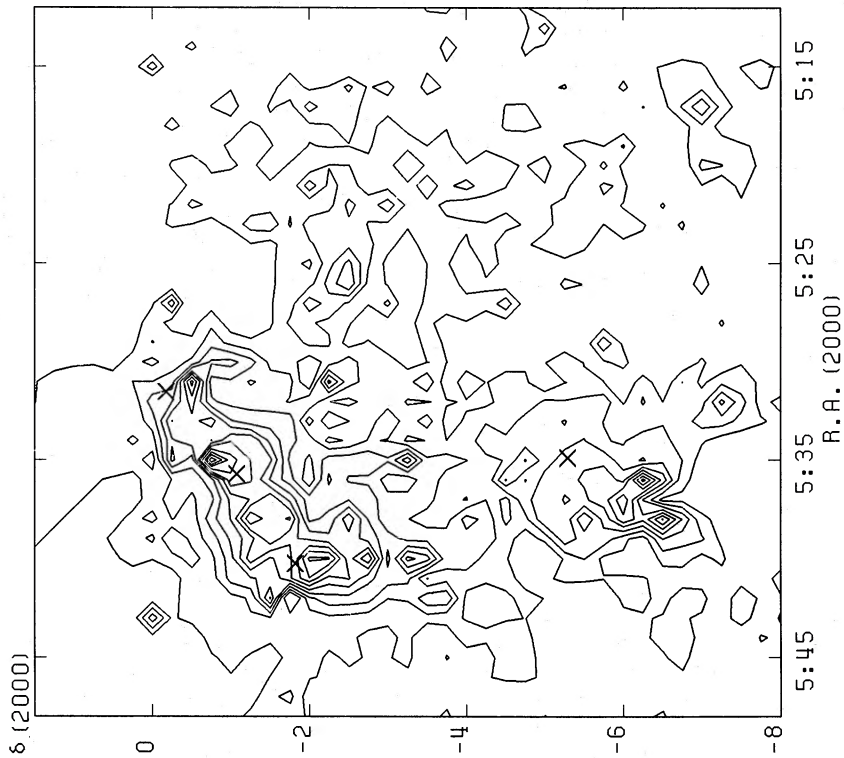

FIG. 1c

of the instrumentation and the rocket flight are given in Paper I, together with a description of the absolute calibration.

After removal of stellar signals, the data were integrated over three raster scans to yield the mean surface brightness for each pixel of 1 min × 0°.25. Because of the incompleteness of the raster-scan-path coverage or because of the subtraction of stellar signals, some pixels lack accurate data. A surface brightness value for such a pixel was obtained from interpolation. Contour maps were then drawn by smoothing the discrete data. The general background of the signal was determined from the signal levels for the periods when the outer region of the Orion reflection nebulosity was observed before and after the raster-scanning period. This background involves contributions from the diffuse galactic light, the zodiacal light, the airglow, and the dark-current noise of the detector system. The dark-current noise was negligible (Paper I), and the zodiacal light was not important in this wavelength range (Cebula and Feldman 1982). Most of the general background was attributed to the diffuse galactic light.

Only the 132.8 nm band was found to be contaminated significantly by the airglow of O I 130.4 and 135.6 nm. The background count in this band increased with the rocket altitude up to 250 km on the upleg of the flight (time after the launch $T = 223$ s). From this point to the point at 180 km on the downleg ($T = 400$ s), no systematic change of the background level was recognized. At the latter point (180 km), the telescope looked at the outer region of the Orion reflection nebulosity. We assumed that the background level did not change during the period 223 s $< T <$ 400 s, and estimated the upper value of the background level from the data around $T = 400$ s. Only the data from this period were used for the 132.8 nm band, after subtracting the estimated constant background. Because of this contamination, the results obtained for the 132.8 nm band should be given less weight. The contamination may seriously affect the resulting spatial distribution, while the mean flux level is not greatly in error.

In the latter half of the observations ($T > 260$ s) the outputs of the 164.0 nm photometer were severely disturbed by spike noises. We discarded this part of the data. Therefore, the data of this band have statistical errors a little larger than those of the other bands, but these errors do not lead to any significant degradation of the final data.

III. RESULTS

a) Large-Scale Nebulosity

Figures 1*a*–1*d* show contour maps of the Orion reflection nebulosity in the far-ultraviolet region. The nebulosity is bright near Orion's Belt and Sword regions, but the surface brightness decreases gradually away from the Belt region in general. A shallow ridge structure along $\alpha \approx 5^h23^m$ appears in these figures.

Following Witt and Lillie (1978) and MNT, the characteristics of the distributions were deduced from plots of the surface brightness S as a function of the radial distance r from a center of the semicircular enhancement of the nebulosity. The center was chosen to be $\alpha = 5^h34^m$, $\delta = -3°$ (1950.0), adopted by the previous observers. Figures 2*a*–2*d* show the radial distributions obtained by the present observation, together with those by *OAO 2* (Witt and Lillie 1978) and *TD-1* (MNT) where available. The differences in the absolute calibration of each observation system are not taken into account in these figures.

In order to quantify the characteristics of the spatial distribution, we fitted the data between $r = 1°$ and $r = 5°$ in Figure 2 with a power-law distribution, $S \propto r^{-p}$, by a least squares method. The slope index p and the surface brightness $S_{100'}$ at a typical distance $r = 100'$ are the characteristic parameters of the radial distribution. In the interpretation of the nebulosity by dust-scattering models, an effective albedo $S_{100'}/F$, where F is the flux of the illuminating stars observed at the Earth, has more physical meaning than $S_{100'}$ itself (see Witt 1977*a*, *b*).

The spectral fluxes of illuminating sources F were estimated by adding up the contributions from stars belonging to the Orion association, as labeled by Warren and Hesser (1977). Most of the bright stars of the association were observed at the same flight, and the fluxes were taken from our data (Paper I). Only one bright star, σ Ori (O9.5 V), was missed in our observations. We estimated its flux by referring to our data on υ Ori (B0 V) and to the difference between the two stars in the *TD-1* data (Jamar *et al.* 1976).

The wavelength dependence of $S_{100'}/F$ is shown in Figure 3*a*, together with the results of *TD-1*, normalized at 195.1 nm. Errors arise mainly from the uncertainty of the general background. The effective albedo of the dust layer increases a little from 195.1 to 179.6 nm and stays almost constant between 179.6 and 148.4 nm. The data for the shortest wavelength indicate that the effective albedo may increase toward shorter wavelengths (< 140 nm).

Figure 3*b* shows the spectral dependence of the slope index p of the radial distributions. Our results indicate rather constant slopes around $p \approx 0.8$, with a less steep slope at 164.0 nm.

b) Comparison with Previous Observations

The *OAO 2* data were sampled at discrete points, including positions well outside $r = 10°$, and may suffer local fluctuations (Witt and Lillie 1978). The *ANS* data were obtained at discrete points only in the vicinity of ζ Ori (de Boer 1983). The *TD-1* observations scanned the whole Orion region, including the northeast region in addition to the present observational region (MNT). These differences in observational regions must be borne in mind in intercomparison of the data from various sources.

In Figures 2*a* and 2*d*, the *OAO 2* flux levels are systematically higher than the present ones. The *OAO 2* data are uncorrected for the background due to diffuse galactic light and other sources. This, as well as the difference in the absolute calibration (~23% at 155.5 nm and ~3% at 191.5 nm [Paper I]), may account for the excesses. A part of the excess at 155.5 nm may be attributed to the fact that the *OAO 2* flux level at this channel is excessively high for various faint objects (see de Boer 1983). The *TD-1* flux levels are lower than the present ones for both the 155 nm and the 195 nm bands, especially in the outer portion of the nebulosity. This cannot be attributed to the difference in the absolute calibration, which was found to be small in these passbands ($< 15\%$ [Paper I]). In a study of the diffuse scattered light near ζ Ori with *ANS*, de Boer (1983) noted that the flux levels of *TD-1* are about a factor of 3 below those of *ANS* and *OAO 2*. At present, no explanation for these discrepancies is available. The flux levels of *ANS* around ζ Ori are higher both at 155 nm and at 180 nm than the present ones at $r = 100'$ but do not exceed them by more than a factor of 2.

As for the wavelength dependence of the data, the relative change of $S_{100'}/F$ found by *TD-1* agrees in general with the present data. The previous investigators indicated an increase of the slope index p from the near-ultraviolet toward 150 nm

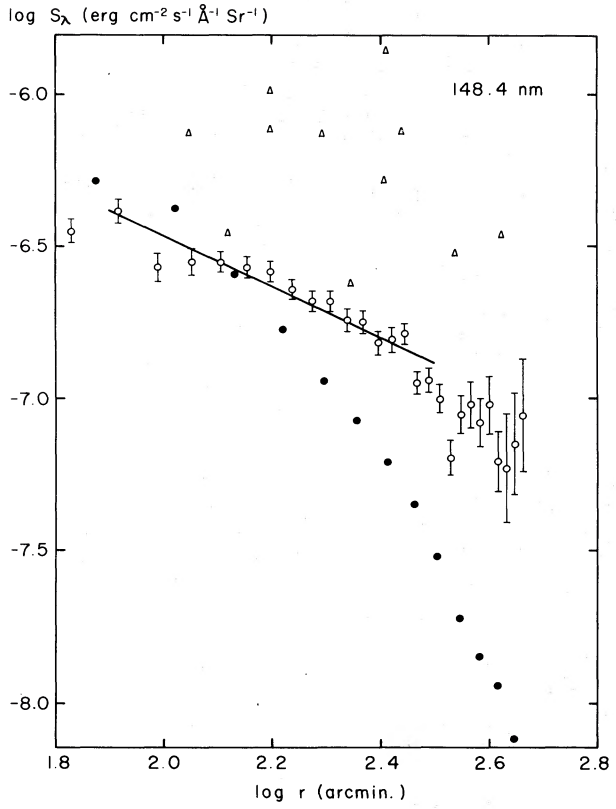

FIG. 2*a*

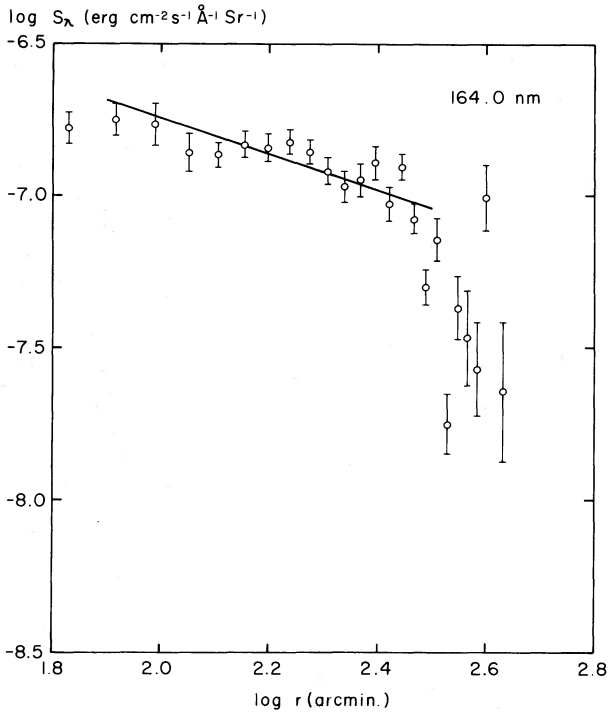

FIG. 2*b*

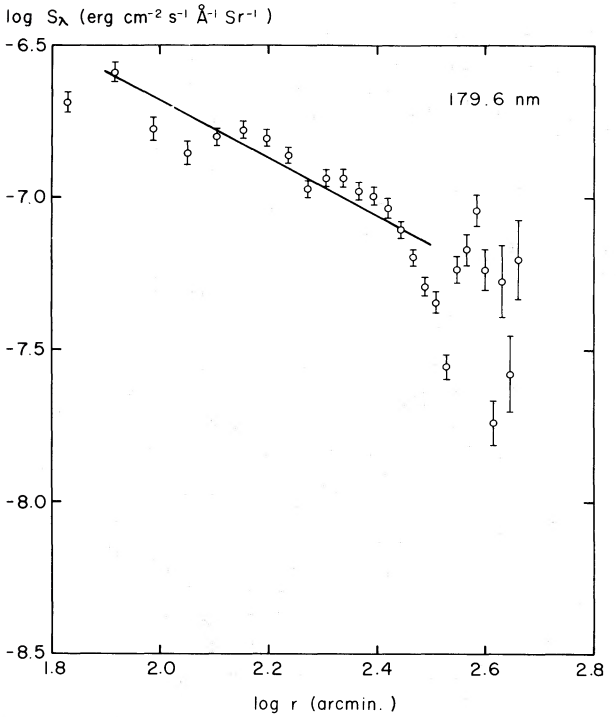

FIG. 2*c*

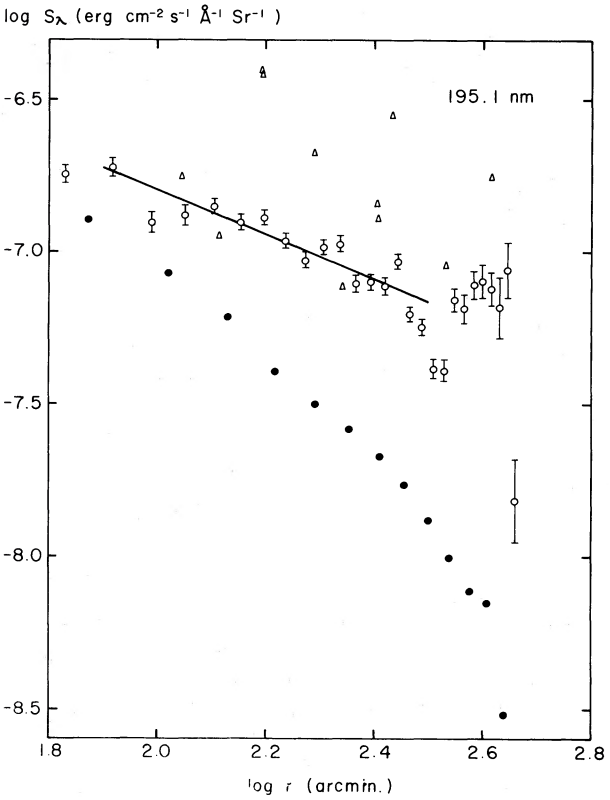

FIG. 2*d*

FIG. 2.—Radial distributions of the nebulosity at (*a*) 148.4 nm, (*b*) 164.0 nm, (*c*) 179.6 nm, and (*d*) 195.1 nm. Least squares fitted lines are also indicated. In Figs. 2*a* and 2*d*, the data of *OAO 2* (155.5 and 191.5 nm [Witt and Lillie 1978]) are plotted as triangles and those of *TD-1* (155 nm and 195 nm [MNT]) as filled circles for comparison.

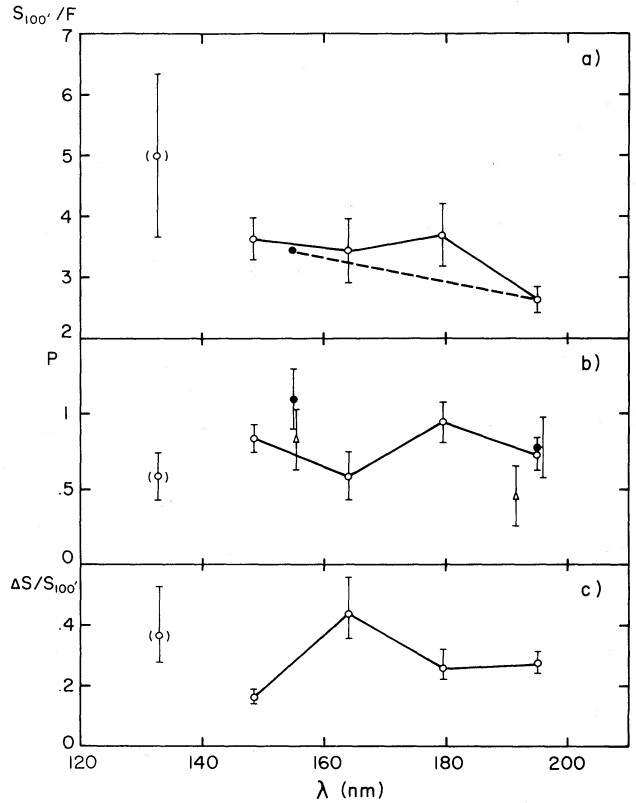

FIG. 3.—(*a*) Ratios of surface brightness at $r = 100'$ to the flux of illuminating stars at the Earth. The data of *TD-1* (MNT), which are normalized at 195 nm, are also shown as filled circles and connected by a dashed line. (*b*) Slopes of the radial distributions. The results of *OAO 2* (Witt and Lillie 1978) and those of *TD-1* (MNT) are also plotted as triangles and filled circles, respectively. (*c*) Mean intensity of the ridge, which is normalized at the surface brightness at $r = 100'$.

(Witt and Lillie 1978; MNT). Within the small wavelength range observed by us the present data do not confirm the increase.

c) Ridge Structure

In order to investigate substructures of the brightness distribution, we subtract the large-scale distribution ($S \propto r^{-p}$) from the original maps and take out the local increments ΔS. The resulting differential map for 148.4 nm is shown in Figure 4 as a typical example. The differential maps for the other bands reveal similar structures. An amorphous ridge structure along $\alpha \approx 5^h23^m$ appears clearly. This ridge corresponds to the western part of the ring structure previously detected in the ultraviolet photograph (220–410 nm [OYH]) and in the maps by the *TD-1* S2/68 telescope down to 150 nm (MNT). The *TD-1* data reveal the whole ring, including the northeast part, which is seen to be bright in Hα. According to their data, the mean ultraviolet intensity of the southwest part is the same as that of the northeast within the observational errors.

The mean intensity of the ridge ΔS was obtained by averaging over the area indicated by a rectangle in Figure 4. Errors in ΔS are estimated to be small ($\pm 2\%$), since the errors due to the uncertainty of the general background are canceled out in the derivation of ΔS. The obtained intensity is consistent with the *TD-1* results in order of magnitude. The ratio of mean intensity of the ridge to the mean surface brightness of the distance $r = 100'$ is plotted in Figure 3*c*. Error bars mainly correspond to the uncertainty of the general background in deriving $S_{100'}$. The observed ratio indicates a small maximum at 164.0 nm and a slight decrease at 148.4 nm.

IV. MODEL CALCULATION

a) Models

Radio observations by Kutner *et al.* (1977) show the existence of a massive molecular cloud complex in the direction of Orion. This complex is believed to be located behind Orion stars. The ultraviolet measurement by *Copernicus* (Cowie, Songaila, and York 1979) indicated that a thick, dense shell of swept-up cloud material is located behind the high-velocity component centered at the Orion OB1 association. The observations of Hα emission by Reynolds and Ogden (1979) also suggested the existence of an expanding shell of the optically emitting gas enclosing the constellations Orion and Eridanus.

In the light of these observations, we adopt a picture of the Orion region such that a deformed spheroidal dust shell encloses the Orion stars and scatters the starlight, producing the observed ultraviolet diffuse light. The emission from the gas may overlap the scattered starlight. The asymmetric distributions of the Barnard Loop in Hα (Isobe 1973) and of the radio continuum (Reich 1978) suggest that the gas-to-dust ratio may be smaller in the southwest part of the Orion region than in the northeast part (see also OYH). Therefore, the area observed by us may provide more favorable conditions than the northeast part for the investigation of the dust shell in the far-ultraviolet. The local increment of ultraviolet intensity in the northwest ridge could be explained by emission from the gas (MNT), but the excess in the southeast ridge, observed in the present study, is not explainable in the same manner, since this part shows neither intense Hα emission nor H I concentration. In our models we attribute the excess in this ridge to the dust scattering of starlight by the sidewall of the spheroidal dust shell.

As a first step in approximating this situation, we simply divide the spheroidal dust shell into three homogeneous slab components: a back slab, a front slab, and a side slab of the dust layer (see Fig. 5). Scattering properties of the front and back slabs are investigated separately in the interpretation of the large-scale nebulosity. Hybrid models including both front and back slabs will be discussed briefly in § IV*f*. Scattered light from the side slab raises the ridge structure. In the following, a model with back and side slabs will be called a back-dust-layer model (BDLM), and a model with front and side slabs a front-dust-layer model (FDLM). Since most of the brightest illuminating stars are concentrated in the Orion Belt region, a point-source approximation is adopted. Effects of the planar extension of illuminating sources will be analyzed in § IV*e*. In these model calculations, only single scattering is taken into account, because our observed area is limited to a relatively inner part of the nebulosity ($r < 10°$). Multiple scattering becomes important only in the outer region (Witt and Oshel 1977).

The scattering phase function $\Phi(\theta, g)$ is taken to be the Henyey-Greenstein function (Henyey and Greenstein 1941), where θ is the scattering angle and g the asymmetry factor. The ratio of the surface brightness S at a radial distance r to the source flux F at the Earth is given for single scattering by

$$S(r)/F = \int_{z_m}^{z_M} \gamma\Phi(\theta, g) \exp(-\tau)\beta/(z^2 + r^2)dz ,$$

where γ is the albedo for single scattering and τ is the optical

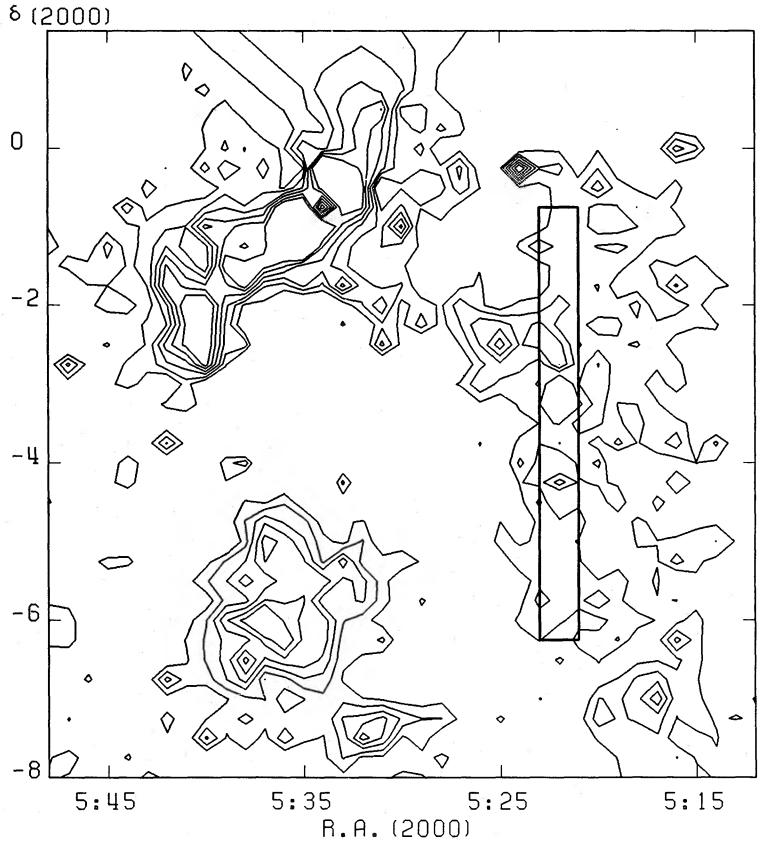

FIG. 4.—Contour maps of the ridge structure for 148.4 nm. Contours run in increments of 1×10^{-7} ergs cm^{-2} sec^{-1} sr^{-1} Å^{-1} from zero. The area indicated by a rectangle was averaged over to obtain the mean intensity of the ridge.

depth of the light path. Details of calculation are given in the Appendix. The integration is to be carried out along the line of sight z. The integration limits z_M and z_m depend on the assumed geometry. The distance variables r and z are normalized by the distance from the Earth to the Orion region ($\sim$450 pc). The radius of the observed ring is about 0.1 in these units. The parameter β determines the geometrical thickness of the dust layer if the optical depth of the layer, τ_0, is given (see eq. [A3]). In the following calculations, we assume $\beta = 400$, which corresponds to assuming the geometrical thickness of the layer to be about $1.1\tau_0$ pc. The results are almost insensitive to the choice of β between 100 and 2000.

We fix the optical thickness of the back slab at unity ($\tau_0 = 1$). The scattering property depends only weakly on τ_0 when multiple scattering is neglected and $\tau_0 > 1$. Then the free parameters determining the back-slab scattering are the albedo for single scattering, γ; the asymmetry factor g; and the distance d between the back slab and the illuminating source in the

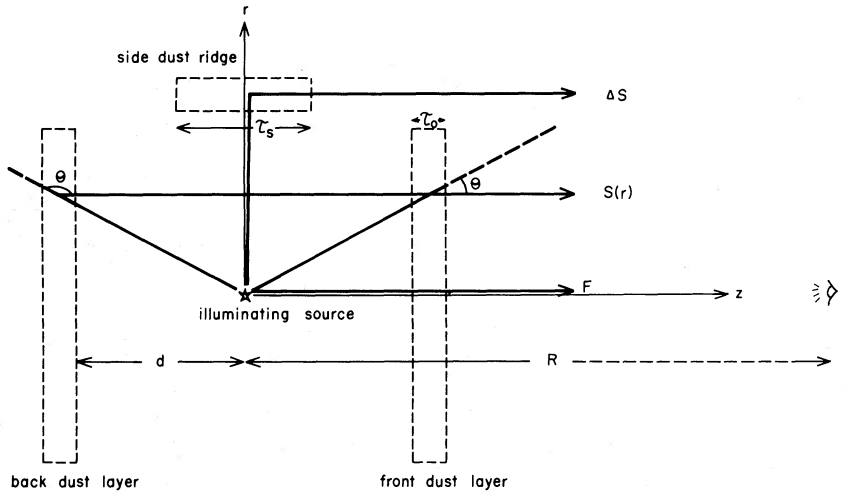

FIG. 5.—The schematic model geometry

adopted units. In most calculations of the front slab, we fix d at 0.1, equal to the radius of the observed ring structure. Effects of the distance will be discussed shortly. Stars in the Orion region are reddened about 0.05 mag in $E(B-V)$ as an average. According to the average interstellar extinction curve (Savage and Mathis 1979), the optical depth in the far-ultraviolet region is about 0.5, although the relevance of the average curve for the Orion region is subject to question. We assume only $\tau_0 < 1$ and take τ_0 to be a free parameter. The other free parameters for the front slab are the albedo γ and the asymmetry factor g. It is assumed that the side slab is located at a distance of 0.1 in units of distance from the source and that the optical thickness of the slab in the line of sight is larger than unity. The dust-scattering parameters γ and g are then the only free parameters in the calculation of the side-slab scattering. The optical quantities, such as γ, g, and τ_0, are functions of the wavelength, and their properties will be discussed in § V*b*.

b) *Back Slab*

The previous investigators assumed the back-slab geometry (Witt and Lillie 1978; MNT), but the details of model calculations were not reported for the Orion reflection nebulosity. Results of our calculation are shown in Figure 6*a*. We plot $(S_{100'}/F)/\gamma$ and p for each model with different d and g to construct a model grid. It is obvious from Figure 6*a* that the slope p depends strongly on the choice of the distance d between the

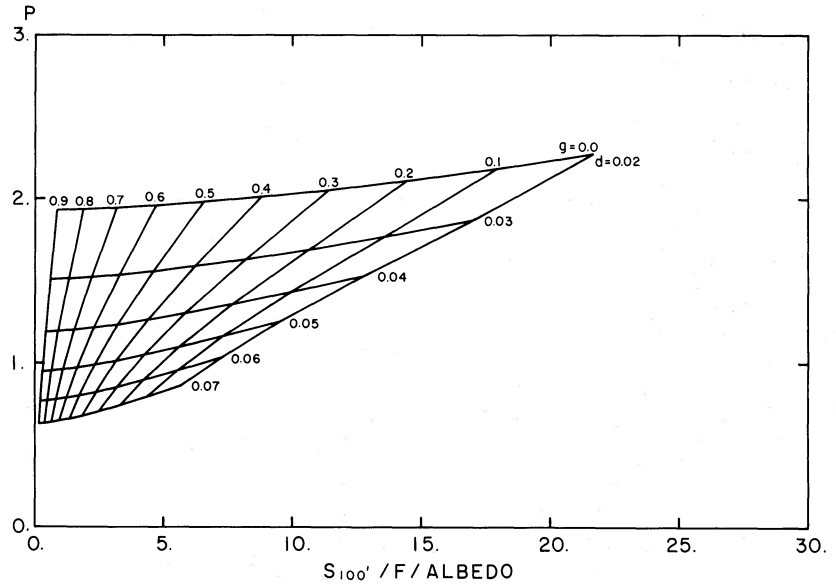

FIG. 6*a*

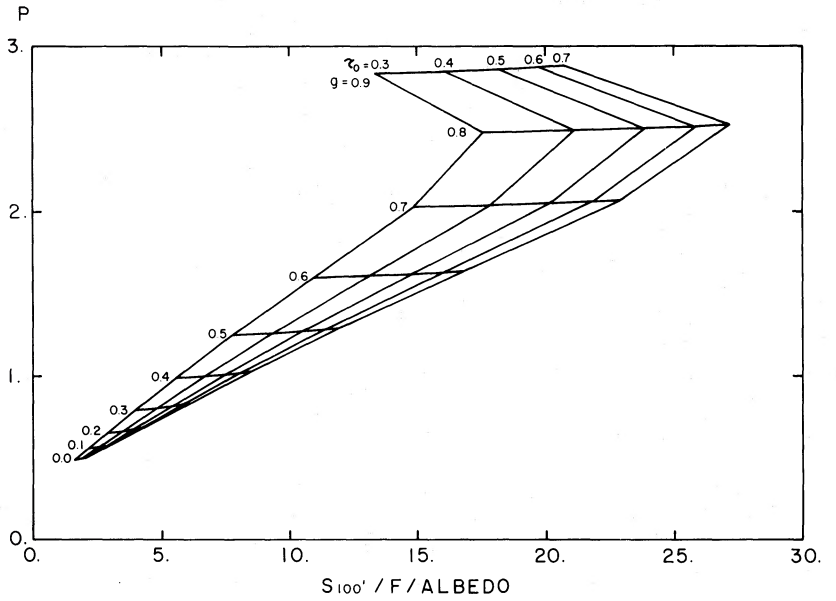

FIG. 6*b*

FIG. 6.—(*a*) Calculation results for back slabs. A grid consists of models with different values of g and d, and $\tau_0 = 1$ (see text). Numbers in the figure indicate these values. The ordinate shows the slope of the calculated distributions between $r = 1°$ and $r = 5°$, and the abscissa indicates the ratios of surface brightness at $r = 100'$ to the flux of illuminating source at the Earth divided by the albedo for single scattering. (*b*) Calculation results for front slabs with $d = 0.1$. Numbers in the figure show the values of g and τ_0 for each model. The ordinate and the abscissa are the same as in Fig. 6*a*.

back slab and the illuminating source, while the asymmetry factor g hardly affects the values of p (see Appendix). Therefore, it is essentially difficult to determine the albedo γ and the asymmetry factor g separately in this geometry only from the observations of p and $S_{100'}/F$. However, this argument is affected by the form of the assumed phase function. The one-term Henyey-Greenstein phase function (OTHG), which has often been employed, is appropriate for studies of scattering situations that are dominated by forward scattering, but it cannot produce the glory phenomenon that results from enhanced scattering amplitudes near $\theta \approx 180°$. For actual dust grains, however, this phenomenon may be suppressed as a result of the irregular shapes of the grains, and the OTHG function may be capable of describing actual scattering situations quite well (Witt 1977*a*).

c) Front Slab

Figure 6*b* shows the model grid for the front slab with varying g and τ_0 as parameters. In this model, the effects of the optical thickness of the slab τ_0 cannot be separated from that of the albedo γ, owing to the nature of the optically thin model. The slope index p of the brightness distribution depends sensitively on the choice of g. The increase of distance d shifts the model grids toward the lower left-hand corner along the line $\tau_0 =$ constant.

d) Side Slab

We adopt a side-slab model for the ridge structure in which the sidewall of the spheroidal dust shell scatters starlight from the center in the perpendicular direction ($\theta \approx 90°$), producing the excess intensity ΔS (Fig. 5). In Figure 7, the ratio of ΔS relative to $S_{100'}$ is plotted as a function of g for the BDLM with $d = 0.05$ and $\tau_0 = 1$ and for the FDLM with $d = 0.1$ and $\tau_0 = 0.5$, assuming that the value of g is common between the side slab and the front/back slab. The ratio of ΔS to $S_{100'}$ of the BDLM has relatively weak dependence on g, while in the FDLM the ratio is quite sensitive to g. As pointed out above, however, the conclusion for the BDLM must be considered tentative because of the ambiguity in the applicability of the OTHG function.

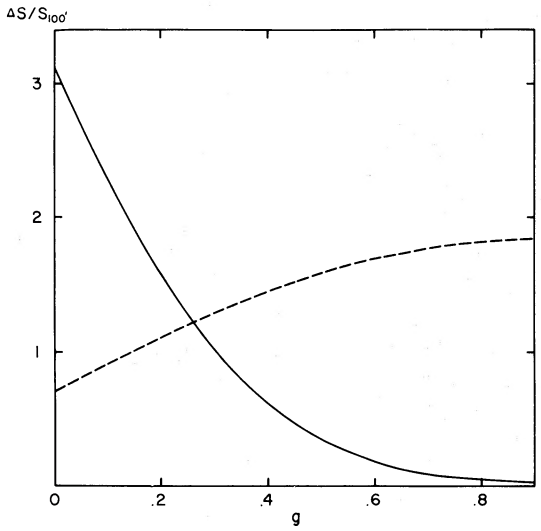

FIG. 7.—Calculated ratios of the ridge intensity (side scattering) to the surface brightness at $r = 100'$, as a function of the asymmetry factor g. The solid line indicates the ratio for the front-dust-layer model (FDLM) with $\tau_0 = 0.5$ and $d = 0.1$, and a dashed line indicates those for the back-dust-layer model (BDLM) with $\tau_0 = 1$ and $d = 0.05$.

e) Multisource Effects

We investigate the multisource situation by taking the actual distribution of plural illuminating sources into account approximately. It is assumed that all the source stars are distributed in a thin layer parallel to the back or the front slab. The extension of the region of distribution of the source stars along the line of sight introduces further complications and is neglected in the present calculations. Results of the calculations including the six brightest stars (ι Ori, ζ Ori, δ Ori, $\theta^{1,2}$ Ori, and ϵ Ori) differ from those adding the next five brightest stars (σ Ori, υ Ori, η Ori, 42 Ori, and HD 36960) only by 3% at most in $S_{100'}/F$ and p. Also, differences in color of the stars do not introduce more than $\pm 2\%$ differences in $S_{100'}/F$ and p. Accordingly, the following discussion refers to the six-star case.

In the case of the back slab, the multisource calculation gives smaller values of $S_{100'}/F$ by 20% on an average and by 25% at most, and of p by 25% on an average and by 30% at most, than the point-source calculation depending on the distance d. From Figure 6*a*, therefore, the point-source calculation with the distance d is almost equivalent to the multisource calculation with the distance $d - 0.01$ in general. As for the front slab, the amount of the multisource effects on $S_{100'}/F$ and p is almost same as for the back slab if $g < 0.9$. In this case, therefore, the point-source approximation provides values of g less by about 0.1 than the multisource model according to Figure 6*b*.

Only the difference of geometrical dilution among multiple sources is important for the scattering property of the side slab. The difference in ΔS between the point-source and the multisource calculations is estimated to be 4% at most. The value of $\Delta S/S_{100'}$ increases by 25% on an average and by 30% at most for both the BDLM and the FDLM because of the decrease of $S_{100'}$ when multiple sources are included. It is concluded that the general trends discussed in §§ IV*b*–IV*d* or seen in Figures 6*a*, 6*b*, and 7 are almost unchanged even if the planar distribution of illuminating sources is taken into account.

f) Hybrid Effects

We investigate hybrid cases taking account of both the back and the front dust slabs simultaneously, assuming that the dust-scattering parameters γ and g are the same in both slabs. We neglect the interaction between two slabs in accordance with the single-scattering approximation and simply examine the relative contributions from the two slabs.

From Figures 6*a* and 6*b*, we find that when the distance $d(B)$ of the back slab becomes larger, the importance of the front slab increases, and that when the asymmetry factor g or the optical thickness of the front slab $\tau_0(F)$ decreases, the importance of the back slab increases in its contribution. With $\tau_0(F) > 0.3$, and $d(B) > 0.07$, $S_{100'}$ of the back slab is less than 30% of that of the front slab for $g > 0.4$, while with $\tau_0(F) < 0.7$ and $d(B) < 0.03$, $S_{100'}$ of the front slab is less than 30% of that of the back slab for $g < 0.1$. In these cases, hybrid effects induced by the addition of a minor contributor decrease the slope index p and increase the effective albedo $S_{100'}/F$ in comparison with single-slab cases. For $g = 0.4$, the back slab with $\tau_0 = 1$ and $d = 0.03$ gives almost the same value of $S_{100'}$ as does the front slab with $\tau_0 = 0.3$ and $d = 0.1$.

In the case of multiple sources, the back slab gives a smaller distance $d(B)$ and the front slab a larger asymmetry factor g

than in the case of a point-source approximation that provides equivalent $S_{100'}/F$ and p. Therefore, the above argument concerning hybrid cases is still valid even quantitatively when the planar extension of the illuminating source is taken into account.

V. DISCUSSION

It is difficult in general to derive the scattering properties of dust uniquely from observations of scattered light alone, since interpretations depend strongly on the assumed geometry (Jura 1979; Cottrell and Witt 1983). The effects of the geometry and the scattering parameters, such as the asymmetry factor g and the albedo γ, cannot be easily decoupled in the analysis. To reduce these uncertainties, infrared observations provide useful information, since they impose a restriction on the possible value of the albedo independent of other parameters (see Witt *et al.* 1982). The present study provides two additional pieces of information not given by the previous observations. The medium spectral resolution of the present photometer marginally detected small spectral changes in p and $\Delta S/S_{100'}$ at 164.0 nm. This must be accounted for consistently in the model calculations, if confirmed by further observations. The assumption of a spheroidal dust shell provides information on two different geometries: backward/forward scattering and sideward scattering. There are three observational quantities available: $S_{100'}/F$, p, and $\Delta S/S_{100'}$. In the following, we derive the scattering properties of dust grains by comparing the observed quantities with the model calculation.

a) *Ranges of Dust-scattering Parameters*

We first estimate the ranges of absolute values of parameters commanding scattering processes, ignoring their wavelength dependence. The estimates should be regarded as indicative rather than as decisive, because we made various assumptions to simplify the analysis. Both the BDLM (d, g, γ) and the FDLM (τ_0, g, γ) have three free parameters each, which can be determined by the observation of p, $S_{100'}/F$, and $\Delta S/S_{100'}$. The observed values are $p = 0.6$–1.0, $S_{100'}/F = 2.5$–4.0, and $\Delta S/S_{100'} = 0.1$–0.5.

In the BDLM the range of d is fixed by p almost irrespective of g and γ, being between 0.05 and 0.08. The value of g can be determined from $\Delta S/S_{100'}$ with the determined d, and the value of γ from $S_{100'}/F$ with the determined d and g. However, $\Delta S/S_{100'}$ in the BDLM calculation is always larger than the observed values when $g > 0$ (see Appendix). There is no solution for g in this case. If some contribution from the front slab [$\tau_0(F) < 0.5$] is added, the BDLM with $d = 0.04$, $g = 0$, and $\gamma < 0.3$ may be compatible with the observational results as a marginal case. Improvement of the form of the scattering phase function may resolve the problem.

In the FDLM, the radial gradient p determines the range of the asymmetry factor g as $0.1 < g < 0.4$, regardless of τ_0 and γ. The value of τ_0 can be obtained from $\Delta S/S_{100'}$ with the determined g, being greater than 0.7 for $g > 0.3$. For $g < 0.3$, the value of $\Delta S/S_{100'}$ in the FDLM calculation is too large to be compared with the observation. The albedo γ is found to be between 0.3 and 0.6 from the observed values of $S_{100'}/F$ with the obtained g and τ_0. The contribution of the back slab is less than 30% of that of the front slab with the parameters if $d(B) > 0.08$.

If the extension of the planar distribution of the source is taken into account, the value of d in the BDLM and that of g in the FDLM will be changed slightly according to § IV*e* ($0.2 < g < 0.5$ for the FDLM and $0.04 < d < 0.07$ for the BDLM), but the others will be almost unchanged.

b) *Spectral Variations of Dust-scattering Parameters*

We now discuss the spectral variations of the scattering parameters by taking the dependence of the observed quantities upon the wavelength into account. The relative spectral changes of the parameters are more accurate and more significant than the individual absolute values.

The BDLM has difficulty in reproducing the small dip of p at 164.0 nm. In this model the slope index p is determined mainly by d, and an unreasonably large decrement of g is required if the dip is accounted for by the variation of g. Since the simple assumptions, including the form of the scattering phase function, may be crucial in the BDLM analysis, the BDLM should not be ruled out simply by this fault.

In the FDLM, the dip of p and the increment of $\Delta S/S_{100'}$ at 164.0 nm can be explained as a decrement of g ($\Delta g \approx -0.1$), while g must be almost constant for the other bands. From the spectral variations of $\Delta S/S_{100'}$ and g, the optical thickness τ_0 of the front slab is required to have no appreciable change from 195.1 to 164.0 nm and an increase greater than 0.1 at 148.4 nm. The spectral change of the albedo γ is obtained from the observed $S_{100'}/F$, and g and τ_0 determined above, showing a continuous increase from 195.1 to 164.0 nm ($\Delta\gamma \approx 0.2$) and a decrease at 148.4 nm ($\Delta\gamma \approx -0.1$). The FDLM can provide a more consistent set of the scattering parameters than the BDLM to explain the spectral variations of the observational results.

c) *Comparison with Previous Analyses*

The previous interpretation of the Orion reflection nebulosity in terms of the back slab including multiple scattering indicated a less forward-throwing character of the scattering function around 150 nm than in the near-ultraviolet region (Witt and Lillie 1978; MNT). The present analysis did not deduce the previous indication within the narrow wavelength range either by the BDLM or by the FDLM. In the BDLM, nearly isotropic scattering within the wavelength range observed by us is suggested from $\Delta S/S_{100'}$. In the FDLM, it is suggested that the asymmetry factor remains rather constant over the observed wavelength range, with a hump at 164.0 nm.

Observations of the high-latitude diffuse galactic light by *Apollo 17* indicate strongly forward-throwing scattering properties of interstellar grains at 150 nm ($g > 0.7$) (Henry *et al.* 1978; Henry 1981; Anderson, Henry, and Fastie 1982), although those observational results are not confirmed by other investigators (see Paresce and Jacobsen 1980; Paresce, Jacobsen, and Bowyer 1983). Such a large value of g is not allowed by the constraint set by the slope index p in the present model analysis of the Orion diffuse light. A slightly smaller g-value ($g = 0.7 \pm 0.1$) indicated by the *OAO 2* observations of the diffuse galactic light (Lillie and Witt 1976) is still a little larger than the upper limit of g in the FDLM, taking account of the extension of illuminating sources.

The observations of the Merope nebula by Witt (1977*c*) indicated $g(155\text{ nm}) \approx 0.25$ and $g(180\text{ nm}) \approx 0.35$. Comparing them with $g(250\text{ nm}) \approx 0.5$, Witt suggested that the scattering phase function is changing to a more isotropic form toward 150 nm. Witt *et al.* (1982) also suggested, on the basis of observation of the reflection nebula NGC 7023, that $g(140\text{ nm}) \approx 0.25$, $g(170\text{ nm}) \approx 0.35$, $g(200\text{ nm}) \approx 0.4$, and $g(250\text{ nm}) \approx 0.5$, supporting the change of the scattering phase function. The study of scattered light around λ Ori by Morgan (1980) did not confirm the decrease of the asymmetry factor from the near-ultraviolet to the vacuum ultraviolet regions,

since the errors prevent an accurate determination of g. The present wavelength range should be wide enough to reveal such an amount of change in g as a change in p in the FDLM analysis, but we cannot confirm the change. The BDLM analysis may not be incompatible with the spectral change of g, although it lacks overall consistency. A typical model of interstellar grains (Mathis, Rumpl, and Nordsieck 1977) predicts an increase of g from 0.55 at 200 nm to 0.63 at 150 nm (White 1979). The present data are not accurate enough to examine a change of this amount.

The spectral variation of $\tau_0(F)$ found in the present study is compatible with the average interstellar extinction curve (Savage and Mathis 1979) in general. The decrement of g and the increment of γ at 164.0 nm, which are suggested by the changes in p and $S_{100'}/F$, is to be investigated in relation to the extinction properties of dust grains. The interstellar extinction curve may actually have a small increment around 160 nm, especially in the Orion-Monoceros region (see Koornneef 1978; Savage and Mathis 1979). Recent investigations by Massa, Savage, and Fitzpatrick (1983) have concluded that the features are probably spurious owing to the mismatch in spectral type of the reddened and unreddened stars. They have also suggested that the extinction curve can be decomposed observationally into two components: a component with an extinction hump at 220 nm and a smooth component with an inverse wavelength dependence (see also Greenberg and Chlewicki 1983). The former component has a minimum extinction around 160 nm, and the latter could be dominant there. Our results, that the scattering is more isotropic at 164.0 nm and that a higher albedo is suggested at 132.8 nm, imply that the latter component is mostly scattering, caused by particles whose radii are less than 50 nm.

VI. SUMMARY

1. The maps of the Orion reflection nebulosity at 195.1, 179.6, 164.0, and 148.4 nm were presented. Large corrections were necessary for the data of 132.8 nm because of the airglow contamination.

2. The ridge structure in the southwest part was revealed clearly after subtraction of the large-scale nebulosity.

3. The analysis of the radial distribution of the nebulosity and the intensity of the ridge structure suggested that the Orion reflection nebulosity can be represented successfully by the starlight scattered by dust grains in a deformed spheroidal shell.

4. The large-scale nebulosity can be explained either by the BDLM or by the FDLM, with preference for the latter.

5. The spectral variations of the asymmetry factor g and the albedo γ were obtained. No positive evidence was obtained that the dust-scattering properties were less forward throwing at 148.4 nm than at 195.1 nm. Nor was a very large value of g (>0.7) indicated around 150 nm. However, regardless of the assumed geometry, the ultraviolet asymmetry factor in Orion is less than the commonly accepted value of the asymmetry factor in the visual region (~ 0.7).

6. The small changes found in the wavelength dependence of the properties of scattered light at 164.0 nm may correspond to the change of the extinction properties of dust grains around these wavelengths.

The authors are deeply grateful for ISAS staff technical support during the rocket experiments. They thank K. Nishi, A. Yamaguchi, M. Nakagiri, and K. Akita of the Tokyo Astronomical Observatory for efficient assistance in the laboratory work, and T. Sasaki and T. Tsujimura of the University of Kyoto for great help during the whole experiment. They also thank R. C. Bless and T. Ogawa for information about the airglow data, A. N. Witt and K. S. de Boer for constructive suggestions on the draft version of this paper, and S. Isobe for various comments. Numerical calculations were carried out at the Computer Center, University of Tokyo.

APPENDIX

In this Appendix we will present a formulation of a single-scattering problem used in our calculations, and give some analytical consequences. The adopted coordinates and geometries are given in Figure 5. We assume a cylindrical symmetry, with the symmetry axis lying along the line of sight. Let r' be the radial coordinate and z' be the coordinate in the direction of the axis, which increases toward the observer. The origin is taken to be at the illuminating source. The surface brightness at r' is obtained by integrating the scattered light along the line of sight z' and is given by

$$S(r') = \int_{z'_m}^{z'_M} R^2(r'^2 + z'^2)^{-1}\gamma F\Phi(\theta, g) \exp(-\tau) n\sigma dz' , \quad \text{(A1)}$$

where F is the flux of illuminating source observed at the Earth and R is the distance between the source and the Earth. The scattering phase function is assumed to be the Henyey-Greenstein function:

$$\Phi(\theta, g) = \pi(1 - g^2)/4(1 + g^2 - 2g\cos\theta)^{3/2} , \quad \text{(A2)}$$

with $\cos\theta = z'/(z'^2 + r'^2)^{1/2}$.

A layer-thickness parameter β can be defined in terms of the scattering cross section σ, the number density n of grains, and R as

$$\beta = n\sigma R . \quad \text{(A3)}$$

If all distance parameters, such as r' and z', are normalized by R, and the prime is dropped for normalized variables, we will obtain an expression for the ratio S/F as given in the text.

The functional form of the optical depth τ, and z_M and z_m, depend on the geometry. Let d be the normalized distance between the source and the dust slab, and τ_0 be the optical thickness of the slab. Then, for the back slab,

$$\tau = \beta[(r^2 + z^2)^{1/2}(z + d)/z - z + d] , \quad \text{(A4)}$$

$$z_M = -d \quad \text{and} \quad z_m = -(d + \tau_0/\beta) ; \quad \text{(A5)}$$

for the front slab,

$$\tau = \beta[(r^2 + z^2)^{1/2}(z - d)/z + z_M - z] , \quad \text{(A6)}$$

$$z_M = d + \tau_0/\beta \quad \text{and} \quad z_m = d ; \quad \text{(A7)}$$

and for the side slab for the ridge structure,

$$\tau = \beta[(r^2 + z^2)^{1/2} - d + z_M - z] , \quad \text{(A8)}$$

$$z_M = \tau_s/2\beta \quad \text{and} \quad z_m = -\tau_s/2\beta , \quad \text{(A9)}$$

where τ_s is the optical thickness of the side slab in the line of sight.

If the geometrical thickness of the dust slab is thin enough, the integration in equation (A1) can be approximated by the value at $z = d$, and we obtain

$$S(r)/F \propto \gamma\Phi(\theta, g)/(r^2 + d^2) . \quad \text{(A10)}$$

If $r \ll d$, which is satisfied in both the back slab and the front slab considered here, then the dependence of $S(r)$ on r is obtained by

$$S(r)/F \propto \Phi(\theta, g)/(r^2 + d^2)$$
$$\propto 1 - [3g/2(1 \pm g)^2 + 1]r^2/d^2 . \quad \text{(A11)}$$

The plus sign is taken for the back slab and the minus sign for the front slab. When g is positive, it is easy to show that $g/(1 + g)^2$ does not vary significantly with g unless g is very small, but $g/(1 - g)^2$ changes drastically with g. Therefore, the slope of the spatial distribution is almost independent of g for the back slab, while it depends strongly on g for the front slab.

The ratio of the excess intensity from the side slab ΔS to the intensity of the back slab or the front slab at $r \approx 0$ is given in the same approximation by

$$\Delta S/S \propto (1 \pm g)^3\tau_s/(1 + g^2)^{3/2}\tau_0 , \quad \text{(A12)}$$

if $\tau_s < 1$ and $\tau_0 < 1$. In the case of $\tau_s > 1$ or $\tau_0 > 1$, τ_s or τ_0 should be replaced by unity. It is obvious that, when $g > 0$, $\Delta S/S > \tau_s/\tau_0$ for the BDLM, and $\Delta S/S < \tau_s/\tau_0$ for the FDLM. In the condition considered here, τ_s and $\tau_0 > 1$ for the BDLM. Therefore, $\Delta S/S > 1$ is an unavoidable result of this model. On the other hand, the FDLM can provide $\Delta S/S < 1$ easily unless τ_0 is unreasonably small. In the BDLM $\Delta S/S_{100}$, has weaker dependence on g than in the FDLM.

REFERENCES

Aannestad, P. A., and Greenberg, J. M. 1983, *Ap. J.*, **272**, 551.
Anderson, R. C., Henry, R. C., and Fastie, W. G. 1982, *Ap. J.*, **259**, 573.
Carruthers, G. R., and Opal, C. B. 1977*a*, *Ap. J.* (*Letters*), **212**, L27.
———. 1977*b*, *Ap. J.*, **217**, 95.
Cebula, R. P., and Feldman, P. D. 1982, *Ap. J.*, **263**, 987.
Cottrell, M. J., and Witt, A. N. 1983, *A.J.*, **88**, 418.
Cowie, L. L., Songaila, A., and York, D. G. 1979, *Ap. J.*, **230**, 469.
de Boer, K. S. 1983, *Astr. Ap.*, **125**, 258.
Greenberg, J. M., and Chlewicki, G. 1983, *Ap. J.*, **272**, 563.
Henry, R. C. 1981, *Ap. J.* (*Letters*), **244**, L69.
Henry, R. C., Anderson, R., Feldman, P. D., and Fastie, W. G. 1978, *Ap. J.*, **222**, 902.
Henyey, L. G., and Greenstein, J. L. 1941, *Ap. J.*, **93**, 70.
Hong, S. S., and Greenberg, J. M. 1978, *Astr. Ap.*, **70**, 695.
———. 1979, *Astr. Ap.*, **88**, 194.
Isobe, S. 1973, in *IAU Symposium 52, Interstellar Dust and Related Topics*, ed. J. M. Greenberg and H. C. van de Hulst (Dordrecht: Reidel), p. 433.
Jamar, C., Macau-Hercot, D., Monflis, A., Thompson, G. I., Houziaux, L., and Wilson, R. 1976, *Ultraviolet Bright-Star Spectrophotometric Catalogue* (ESA SR-27).
Jura, M. 1979, *Ap. J.*, **231**, 732.
Koornneef, J. 1978, *Astr. Ap.*, **68**, 139.
Kutner, M. L., Tucker, K. D., Chin, G., and Thaddeus, P. 1977, *Ap. J.*, **215**, 521.
Lillie, C. F., and Witt, A. N. 1976, *Ap. J.*, **208**, 64.
Martin, P. G. 1972, *M.N.R.A.S.*, **159**, 179.
Massa, D., Savage, B. D., and Fitzpatrick, E. L. 1983, *Ap. J.*, **266**, 662.
Mathis, J. S., Rumpl, W., and Nordsieck, K. H. 1977, *Ap. J.*, **217**, 425.
Morgan, D. H. 1980, *M.N.R.A.S.*, **190**, 825.
Morgan, D. H., Nandy, K., and Thompson, G. I. 1982, *M.N.R.A.S.*, **199**, 399 (MNT).
O'Dell, C. R., York, D. G., and Henize, K. G. 1967, *Ap. J.*, **150**, 835 (OYH).
Paresce, F., and Jacobsen, P. 1980, *Nature*, **288**, 119.
Paresce, F., Jacobsen, P., and Bowyer, S. 1983, *Astr. Ap.*, **124**, 300.
Reich, W. 1978, *Astr. Ap.*, **64**, 407.
Reynolds, R. J., and Ogden, P. M. 1979, *Ap. J.*, **229**, 942.
Savage, B. D., and Mathis, J. S. 1979, *Ann. Rev. Astr. Ap.*, **17**, 73.
Tanaka, W., Onaka, T., Sawamura, M., Watanabe, T., Kodaira, K., and Nishi, K. 1984, *Ap. J.*, **280**, 213.
Warren, W. H., and Hesser, J. E. 1977, *Ap. J. Suppl.*, **34**, 115.
White, R. L. 1979, *Ap. J.*, **229**, 954.
Witt, A. N. 1977*a*, *Ap. J. Suppl.*, **35**, 7.
———. 1977*b*, *Ap. J. Suppl.*, **35**, 21.
———. 1977*c*, *Pub. A.S.P.*, **89**, 750.
Witt, A. N., and Lillie, C. F. 1978, *Ap. J.*, **222**, 909.
Witt, A. N., and Oshel, E. R. 1977, *Ap. J. Suppl.*, **35**, 31.
Witt, A. N., Walker, G. A. H., Bohlin, R. C., and Stecher, T. P. 1982, *Ap. J.*, **261**, 492.

KEIICHI KODAIRA and TETSUYA WATANABE: Tokyo Astronomical Observatory, University of Tokyo, Mitaka, Tokyo 181, Japan

TAKASHI ONAKA, MINEO SAWAMURA, and WATARU TANAKA: Department of Astronomy, Faculty of Science, University of Tokyo, Bunkyo-ku, Tokyo 113, Japan